Photoproduction of mesons in nuclei

at GeV energies [*]

M. Effenberger and U. Mosel

Institut für Theoretische Physik, Universität Giessen

D-35392 Giessen, Germany

UGI-99-21

Abstract

In a transport model that combines initial state interactions of the photon with final state interactions of the produced particles we present a calculation of inclusive photoproduction of mesons in nuclei in the energy range from 1 to 7 GeV. We give predictions for the photoproduction cross sections of pions, etas, kaons, antikaons, and $\pi^+\pi^-$ invariant mass spectra in ^{12}C and ^{208}Pb. The effects of nuclear shadowing and final state interaction of the produced particles are discussed in detail.

I. INTRODUCTION

Photoproduction of mesons in nuclei offers the possibility to study the interaction of photons with nucleons in the nuclear medium. In the total photonuclear absorption cross section one observes experimentally for photon energies above 1 GeV a reduction of the absorption strength in nuclei which is known as shadowing effect. While Vector Meson Dominance (VMD) models are able to quantitatively describe this effect for photon energies above about 4 GeV they usually underestimate the effect for lower photon energies (see e.g. Ref. [1]). In Ref. [2] it has been speculated that this may be related to a decrease of the ρ-meson mass in the nuclear medium.

The in-medium properties of the ρ-meson have found widespread interest during the past decade as they may be related to chiral symmetry [3,4]. The experimental data on dilepton production in nucleus-nucleus collisions at SPS energies [5,6] also seem to indicate a change of the ρ-meson spectral function (lowering of the mass or broadening) in the nuclear medium [7,8].

A third experimental observation that may be related to in-medium properties of the ρ-meson is the disappearance of the $D_{13}(1520)$-resonance in the total photoabsorption cross section in nuclei at photon energies around 800 MeV. In Refs. [9,10] it has been proposed that this disappearance is caused by the large coupling of the D_{13} to the $N\rho$-channel and a medium modification of the spectral function of the ρ-meson.

While a consistent theoretical descriptions of these observations is not yet available our transport approach is a first step into this direction. During the past years we have developed a semi-classical BUU transport model that allows us to calculate inclusive particle production in heavy-ion collisions from 200 AMeV to 200 AGeV, in photon, and in pion induced reactions with the very same physical input. This model has already been very successfully applied to the description of heavy-ion collisions at SIS energies [11,12] and photoproduction of pions and etas up to 800 MeV [13]. Just recently we have given predictions for dilepton production in pion-nucleus reactions [14], that will be measured by the HADES collaboration at GSI [15], and in photon-nucleus reaction in the energy range from 800 MeV to 2.2 GeV [16] that is accessible at TJNAF [17]. In these studies we have investigated direct observable consequences of medium modifications of the vector mesons through their dilepton decay.

The calculation of photoproduction in the region of the nucleon resonances (up to photon energies of about 1 GeV) has recently been extended to electroproduction [18]. In this study we have also discussed different scenarios that might lead to a disappearance of the D_{13} in the total photoabsorption cross section with respect to their influence on more exclusive observables.

It is the purpose of the present paper to give predictions for pion, eta, kaon, and antikaon production in photon-nucleus reactions in the energy range from 1 to 7 GeV. A comparison of these calculations with experiments that are possible at ELSA and TJNAF will on the one hand help to improve our understanding of the onset of the shadowing effect. On the other hand is photoproduction an excellent tool to study medium modifications of the produced mesons since the final observables get strongly modified by the final state interaction of the primary produced particles with the nuclear medium. In photon-nucleus reactions the produced particles have in general larger momenta with respect to the nuclear environment than in heavy-ion collisions. Therefore, photonuclear experiments yield partly complementary in-

formation about the in-medium self energies of mesons compared to heavy-ion experiments. They also have the great advantage that they allow to study the properties of the produced hadrons in an environment that is much closer to equilibrium than in a heavy-ion collision.

While the early seventies have already seen a remarkable number of experimental and theoretical studies of photoinduced particle production (for a rather complete review see Ref. [19]) the emphasis there was on the study of coherent production processes. Incoherent production had to rely for an interpretation on the Glauber approximation that involves a number of approximations and restrictions. The study described here is free of most of these and thus provides a more reliable framework for an interpretations of such reactions. Unfortunately, the few existing experimental data in Refs. [20–22] on incoherent photoproduction of mesons in nuclei were all obtained under very restrictive experimental conditions which, furthermore, can not be reconstructed from the literature. We can, therefore, not compare our results to any data.

Our paper is organized as follows: In Section II we describe briefly the BUU transport model. In Section III we discuss our treatment of elementary photon-nucleon collisions and, in particular, the implementation of the shadowing effect. Our results for photoproduction of pions, etas, kaons, and antikaons are presented in Section IV. We close with a summary in Section V.

II. THE BUU MODEL

We use a semi-classical transport model (BUU) for a description of the final state interactions (fsi) of the produced particles. This description allows a full coupled channel treatment of the fsi, including non-forward processes. Our model has been described in Ref. [16]. Therefore we restrict here ourselves to a brief presentation of the basic ideas and only discuss in detail the basic new features of our method.

The BUU equation describes the classical time evolution of a many-particle system under the influence of a self-consistent mean field potential and a collision term. For the case of identical particles it is given by:

$$\left(\frac{\partial}{\partial t} + \frac{\partial H}{\partial \vec{p}}\frac{\partial}{\partial \vec{r}} - \frac{\partial H}{\partial \vec{r}}\frac{\partial}{\partial \vec{p}}\right)f = I_{coll}[f] \quad , \tag{1}$$

where $f(\vec{r}, \vec{p}, t)$ denotes the one-particle phase space density with $\vec{r}$ and $\vec{p}$ being the spatial and momentum coordinates of the particle. I_{coll} is the collision term and $H(\vec{r}, \vec{p}, f)$ stands for the single particle mean field Hamilton function which, in our numerical realization [11], is given as:

$$H = \sqrt{(\mu + S)^2 + \vec{p}^2} \quad , \tag{2}$$

where $S(\vec{r}, \vec{p}, f)$ is an effective scalar potential. For a system of non-identical particles one gets an equation for each particle species that is coupled to all others by the collision term and/or the mean field potential. Besides the nucleon we take into account all nucleonic resonances that are rated with at least 2 stars in Ref. [23]: $P_{33}(1232)$, $P_{11}(1440)$, $D_{13}(1520)$, $S_{11}(1535)$, $P_{33}(1600)$, $S_{31}(1620)$, $S_{11}(1650)$, $D_{15}(1675)$, $F_{15}(1680)$, $P_{13}(1879)$, $S_{31}(1900)$, $F_{35}(1905)$, $P_{31}(1910)$, $D_{35}(1930)$, $F_{37}(19$

50), $F_{17}(1990)$, $G_{17}(2190)$, $D_{35}(2350)$. The resonances couple to the following channels: $N\pi$, $N\eta$, $N\omega$, ΛK, $\Delta(1232)\pi$, $N\rho$, $N\sigma$, $N(1440)\pi$, $\Delta(1232)\rho$.

We also propagate explicitly the following baryonic resonances with total strangeness $S = -1$: Λ, Σ, $\Sigma(1385)$, $\Lambda(1405)$, $\Lambda(1520)$, $\Lambda(1600)$, $\Sigma(1660)$, $\Lambda(1670)$, $\Sigma(1670)$, $\Lambda(1690)$, $\Sigma(1750)$, $\Sigma(1775)$, $\Lambda(1800)$, $\Lambda(1810)$, $\Lambda(1820)$, $\Lambda(1830)$, $\Lambda(1890)$, $\Sigma(1915)$, $\Sigma(2030)$, $\Lambda(2100)$, $\Lambda(2110)$. The parameters of these resonances are consistent with the values given by the PDG [24] and are listed in Table I. The resonances couple to the channels: $\Lambda\pi$, $\Sigma\pi$, $\Sigma(1385)\pi$, $\Lambda\eta$, $N\bar{K}^*(892)$, $\Lambda(1520)\pi$. The mass dependence of the partial decay widths is treated analogous to the case of the nucleonic resonances (see Ref. [16]); in cases when the relative angular momentum of the decay products is not uniquely given by the quantum numbers we use the lowest possible one. In the mesonic sector we take into account the following particles: π, η, ρ, ω, σ, ϕ, K, $\bar{K}$, $K^*(892)$, $\bar{K}^*(892)$.

For a detailed description of the used cross sections in the non-strange sector we refer to Refs. [16,11]. Baryon-baryon collisions above invariant energies of 2.6 GeV and meson-baryon collisions above 2.2 GeV are described by using the string fragmentation model FRITIOF [25]. For strangeness production in low energy pion-nucleon collisions we adopt the parameterizations for $\pi N \to \Lambda K$ and $\pi N \to \Sigma K$ from Ref. [26] and for $\pi N \to N K \bar{K}$ from Ref. [27]. Strangeness production in baryon-baryon collisions is only of minor importance for the calculations presented here and is described in Ref. [28]. The cross sections for the interactions of kaons and antikaons with nucleons can be found in Appendix A.

III. PHOTON-NUCLEON INTERACTION

In Refs. [16,13] we have described in detail how we calculate photonuclear reactions. The total cross section for any observable is given as an incoherent sum over the contributions from all nucleons in the nucleus where the final state interactions of the particles produced in the primary γN collisions are calculated using the transport equation (1). For invariant energies below 2.1 GeV (corresponding to $E_\gamma = 1.88$ on a free nucleon at rest) we describe elementary γN collisions as in Ref. [13] by an explicit calculation of the cross sections for production of nucleonic resonances as well as one-pion, two-pion, eta, vector meson, and strangeness production. For larger energies we use the string fragmentation model FRITIOF [25] where we initialize a zero mass ρ^0-meson for the photon following a VMD picture. In Fig. 1 we show that this procedure gives an excellent description of charged particle multiplicities in photon-proton collisions. The agreement seen there is better than could be expected from a model that had been developed for applications at higher energies. However, we do not expect the Lund model to give correct predictions for all specific channels, especially with respect to isospin. Since in the Lund model flavor exchange mechanisms are not included processes like, e.g. $\rho N \to \Lambda K$, are not possible. Therefore we treat exclusive strangeness production independent of the Lund model also for energies above the string threshold. The used cross sections for exclusive strangeness production are discussed in Appendix B.

Nuclear shadowing of the incoming photon is taken into account for photon energies above 1 GeV by adopting the model of Ref. [19] in the following way. For the total photon-

nucleus cross section we have:

$$\sigma_{\gamma A} = A\sigma_{\gamma N} - \int d^3 r \rho(\vec{r}) S(\vec{r}) \equiv A_{eff} \sigma_{\gamma N} \quad , \tag{3}$$

where $\rho(\vec{r})$ denotes the nuclear density and $S(\vec{r})$ is given as:

$$S(b,z) = -8\pi \sum_V (T_{\gamma V})^2 \, \mathrm{Im} \left\{ i \int_{-\infty}^z dz' \rho(b,z') \exp\left[iq_{\parallel}^V(z'-z) + 2i\sqrt{\pi}T_{VV} \int_{z'}^z \rho(b,\xi)d\xi \right] \right\} \quad , \tag{4}$$

where we have expressed everything in cylindrical coordinates (b,z) with the photon momentum along the z-axis. The momentum transfer $q_{\parallel}^V$ is:

$$q_{\parallel}^V = E_\gamma - \sqrt{E_\gamma^2 - M_V^2} \quad , \tag{5}$$

with E_γ and M_V denoting the photon energy and the mass of the vector meson V, respectively. In Eq. (4) T_{ab} is the amplitude for the process $aN \to bN$. We used all parameters from [19] (model I) taking into account ρ, ω and ϕ mesons.

In Figs. 2 and 3 the resulting shadowing effect is compared to experimental data as function of photon energy for ^{12}C and ^{208}Pb. Within the experimental error bars the agreement is quite satisfactory.

We can define a shadowing factor $s_N(\vec{r})$ for an in-medium photon-nucleon cross section:

$$s_N(\vec{r}) = 1 - \frac{S(\vec{r})}{\sigma_{\gamma N}} \quad , \tag{6}$$

so that we can write the total photon-nucleus cross section as integral over in-medium shadowed single nucleon cross sections:

$$\sigma_{\gamma A} = \int d^3 r \rho(\vec{r}) s_N(\vec{r}) \sigma_{\gamma N} \quad . \tag{7}$$

In Fig. 4 we show the shadowing factor $s_N(\vec{r})$ for ^{208}Pb at photon energies of 2 and 7 GeV. At 2 GeV there are some interference structures but since s_N varies only between 0.8 and 1.2 the influence of shadowing on our calculations for particle production is very small. At 7 GeV shadowing is much more important. Due to interference effects one sees a rise of s_N for larger z that one naively would not expect.

In our calculations the same shadowing factor $s_N(\vec{r})$ is used for all partial cross sections, so that, for example, the primary in-medium cross section $\sigma_{\gamma N \to Nm}^{med}$ for photoproduction of a meson m in $\gamma N \to Nm$ is related to the vacuum cross section $\sigma_{\gamma N \to Nm}^{vac}$ via:

$$\sigma_{\gamma N \to Nm}^{med} = s_N(\vec{r})\sigma_{\gamma N \to Nm}^{vac}. \tag{8}$$

The final state interactions are then treated in the transporttheoretical framework described in Section II. The initial state interactions of the incoming photon are thus described in a model that contains quantum-mechanical coherence effects whereas the final state interactions are treated in a completely incoherent way.

IV. RESULTS

A. Photoproduction of pions and etas

In Fig. 5 we present the results of our calculations for the total π^- production cross section in ^{12}C (upper part) and ^{208}Pb (lower part). The solid lines display our 'standard' calculations. One sees that the cross section per nucleon is larger for ^{12}C because nuclear shadowing and final state interaction are less effective. For ^{12}C there is also a local maximum around 2 GeV in the excitation function that is not present in ^{208}Pb. This maximum is mainly caused by an interplay of the rising π-production cross section and the onset of shadowing. For ^{208}Pb the decrease between 2 and 3 GeV due to shadowing is neutralized by secondary collisions of the primary produced particles that contribute to the total yield.

For the dashed lines we used a two-body absorption for the $\Delta(1232)$-resonance only instead of the absorption introduced in Ref. [18] that gives an enhanced Δ-absorption. With increasing photon energy the treatment of the Δ-absorption becomes less important. For ^{12}C the improved, new treatment reduces the pion yield by about 5%, for ^{208}Pb by about 20%.

The use of a string fragmentation model in hadronic transport models always requires the introduction of a finite 'formation time'. In our calculations we use $t_f = 0.8$ fm/c (in the rest frame of the produced particles) which leads to a good reproduction of experimental data on pion production in heavy-ion collisions at SPS energies. While this value lies in a reasonable range our formation time prescription is nonetheless questionable as we neglect any interaction of the 'strings' during their formation with the surrounding nuclear medium. From a practical point of view this prescription should thus be regarded as a parameterization of our ignorance with respect to the role of partonic degrees of freedom. In order to explore the resulting uncertainties we have also performed calculations with $t_f = 0$ (dotted lines in Fig. 5). This enhances the final state interactions of the produced particles. Here one should note that by the final state interactions the particle yield is not only reduced but can also be enhanced when a primarily produced particle with high energy strikes another nucleon, as e.g. in $\pi N \rightarrow \pi\pi N$. From Fig. 5 one sees that the formation time becomes more important with increasing photon energy. For ^{12}C the calculation with zero formation time gives an enhancement of the pion yield at 7 GeV by about 15%. This enhancement is less pronounced in ^{208}Pb because the absorption of the secondary produced particles is more effective.

In Fig. 5 we also show results of calculations without shadowing for the incoming photon (dash-dotted lines). Because of the coordinate dependence of the shadowing factor the effect of shadowing is in principle not simply proportional to the effect seen in the total absorption cross section. However, the deviations from this proportionality are quite small as one sees by comparing the results in Fig. 5 to the effective mass numbers in Figs. 2 and 3.

The effect of the final state interaction of the produced particles is, as expected, rather different for ^{12}C and ^{208}Pb. In Fig. 5 calculations without final state interaction are displayed by the dot-dot-dashed lines. Now there are only two competing mechanisms that influence the shape of these excitation functions. On the one hand the particle yield in elementary photon-nucloen collisions increases with photon energy. On the other hand the shadowing effect becomes also more important for higher energies. In the case of ^{208}Pb the shadowing

effect dominates and the cross section decreases monotonously with increasing photon energy. For ^{12}C there is first a decrease of the pion yield up to a photon energy of 3 GeV and then an increase because shadowing is here less important than for ^{208}Pb.

In Fig. 6 we show the effects of the same scenarios on η photoproduction. First one observes a strong increase of the total cross section from 1 to 3 GeV by about a factor of 4 which is simply due to the opening of phase space. The effect of the formation time is again determined by an interplay between secondary production and absorption which results in a very small net effect.

The shadowing effect is, as expected, very similar to the case of pion production. For ^{12}C the calculation without final state interaction gives practically the same result as the 'standard' calculation. This is quite different for ^{208}Pb where the final state interaction reduces the yield, in particular for low photon energies, significantly.

Since the total meson production yield is, as discussed above, determined by different effects that partly cancel each other it is instructive to look at more exclusive observables. In Figs. 7 and 8 we therefore present momentum differential cross sections for the production of pions (upper part) and etas (lower part) at photon energies of 2 and 4 GeV in ^{208}Pb. Here we show our 'standard' calculations (solid lines) as well as calculations without formation time (i.e. maximum final state interaction) (dashed lines) and without final state interaction (dotted lines). In the pion case the spectrum is getting 'softer' with increasing final state interactions.

The η-spectra show a pronounced structure at high momenta that is caused from exclusive processes $\gamma N \rightarrow N\eta$ that are strongly forward peaked. In π^- production such a structure is not present because the string fragmentation model used here does not include flavor exchange mechanisms. We leave the inclusion of such processes for future work. The influence of the final state interaction on the η-spectrum is similar to the pion case: the final state interactions mainly shift the spectrum to lower energies.

In Figs. 9 and 10 we present the results of our calculations for the $\pi^+\pi^-$ invariant mass spectra at photon energies of 2, 4, and 6 GeV in ^{12}C and ^{208}Pb, respectively. We show at each case the total mass differential cross section as well as the contribution coming from ρ^0 decays. The effect of the final state interaction is, as expected, much larger for ^{208}Pb than for ^{12}C. While the peak of the ρ meson clearly dominates the spectrum in ^{12}C it is, especially for low photon energies, harder to identify in ^{208}Pb.

In Ref. [16] we have investigated the observable effects of medium modifications of the vector mesons ρ and ω through their e^+e^- decay in photoproduction at energies between 0.8 and 2.2 GeV. In this study we have found an enhancement of the yield of intermediate mass (~ 500 MeV) dileptons by about a factor 3 when the mass of the ρ meson was reduced in the nuclear medium according to the predictions of Refs. [35,36]:

$$\mu^* = \mu - 0.18 m_\rho^0 \frac{\rho(\vec{r})}{\rho_0}, \tag{9}$$

where m_ρ^0 denotes the pole mass of the ρ meson. In Figs. 9 and 10 the dashed lines show the calculations with such a dropping mass scenario. One sees that the $\pi^+\pi^-$ spectrum is hardly influenced by such a medium modification. This is simply due to the fact that the pions have a very short mean free path in the nuclear medium (~ 1 fm). Therefore the probability that two pions which stem from a decay of a ρ meson at a relevant density are both able to propagate to the vacuum without rescattering is very low.

B. Photoproduction of kaons and antikaons

In Fig. 11 we present our results for K^+-production in ^{12}C and ^{208}Pb. We again show, like for pion and eta production, the results of different model calculations: a 'standard' calculation (solid lines) that includes all effects, a calculation with zero formation time (dashed lines), without shadowing (dotted lines), and without final state interaction (dash-dotted lines). The primary produced $\bar{s}$-quarks can not be annihilated in the nuclear medium and all of them are finally contained in K^+ and K^0 mesons. Therefore the final state interaction can only enhance the K^+ yield. From Fig. 11 one sees that for ^{12}C the number of secondary produced K^+-mesons is almost negligible while for ^{208}Pb they amount to about 30% of the total yield. In a calculation with zero formation time the cross section for K^+ production is enhanced for large photon energies in ^{12}C by about 20% and in ^{208}Pb by about 40%. This enhancement is mainly caused by collisions of primary high energy pions with nucleons. Such pions have a large formation time $t_f^{lab} = \gamma t_f$ in the lab system, where $\gamma = E_\pi/m_\pi$ is a Lorentz factor, which suppresses secondary interactions.

The shadowing effect is very similar to the one for pion or eta production. The fact that the calculations without shadowing and zero formation time are practically identical for both nuclei is accidental.

In Fig. 12 we show our results for K^--production. In contrast to K^+-production primary K^--mesons can be absorbed via processes $K^-N \to Y\pi$. For ^{12}C absorption and secondary production nearly cancel each other as can be seen by comparing the 'standard' calculation (solid line) and the calculation without final state interaction (dash-dotted line). The calcultion with zero formation time gives a slightly larger result. In ^{208}Pb the absorption mechanism is a little more dominant. Therfore, the calculation without final state interaction gives the largest result.

By comparing the total K^+- and K^--production in Figs. 11 and 12 one sees that in our calculation almost as many antikaons as kaons are produced. This is due to the fact that the string fragmentation model produces much more antikaons than hyperons in a ρ^0-nucleon collision which might be an artifact of the model. However, since there are presently no experimental data for inclusive antikaon production in photon-nucleon collisions available it is difficult to check this point. Therefore we stress here that our results for photoproduction in nuclei are only valid under the caveat that our description of the elementary photon-nucleon collision is correct.

In Figs. 13 and 14 we show momentum differential cross sections for production of K^+- and K^--mesons in ^{208}Pb at photon energies of 2 and 4 GeV. The solid lines are our 'standard' calculations, the dashed line are the calculations with zero formation time, and the dotted lines display the result without final state interaction. From the K^+-spectra one sees that the final state interactions primarily enhance the low momentum yield. For the K^--mesons the high momentum tail is significantly reduced by the final state interactions. A comparison of these spectra to future experimental data will therefore be helpful with respect to our understanding of the interactions of kaons with nucleons in the nuclear medium.

V. SUMMARY

We have presented a calculation of photoproduction of pions, etas, kaons, and antikaons in the energy range from 1 to 7 GeV in ^{12}C and ^{208}Pb within a model that contains shadowing of the incoming photon and treats the outgoing particles in a coupled channel semi-classical BUU transport model. It thus goes beyond the standard Glauber treatment because it can describe all possible chains that can lead to the final state under investigation. Predictions for total cross sections as well as momentum differential cross sections were given.

We have investigated in detail the influence of shadowing for the incoming photon and final state interaction of the produced particles on our results. A comparison of experimental data to our results will clarify if our treatment of the in-medium meson-nucleon interactions is correct.

In particular, we have shown that $\pi^+\pi^-$ invariant mass spectra exhibit only a very small sensitivity on medium modifications of the ρ meson.

Our calculations of photoproduction of mesons in nuclei are based on the input of photoproduction of mesons on nucleons for which so far only few experimental data in the relevant energy range exist. New experimental data are urgently needed in order to remove uncertainties coming from the treatment of the elementary process. There are also uncertainties coming from our description of the hadronic interactions because not all channels have yet experimentally been measured or are in principal unmeasurable. However, we do not expect these uncertainties to have a large influence on the results reported here since we have calculated rather inclusive observables for which the total employed cross sections are most decisive.

In assessing the overall reliability of the predictions made here we point out that the method (and code) used here has been shown to provide a very good description of π, 2π and η photoproduction data in the MAMI energy regime (up to 800 MeV) [13,18]. In the present paper we show that the method also describes shadowing very well up to photon energies of a few GeV. The same method also gives an excellent description of meson production in heavy-ion collisions in the GeV regime, typically describing these data within a factor < 2. In these latter reactions the same final state interactions take place as in the present calculation. Thus, both the initial state (shadowing) and the final state interactions with their complex coupled channel effects are well under control. We thus feel confident that the accuracy of the present calculations is as good as that observed in the other reaction channels.

Finally, we wish to mention that the calculations reported here can be extended to the case of electroproduction [18].

APPENDIX A: KAON-NUCLEON AND ANTIKAON-NUCLEON COLLISIONS

The elastic cross section $K^+p \rightarrow K^+p$ is parameterized for invariant energies below the string threshold $\sqrt{s} < 2.2$ GeV by the following expression:

$$\sigma_{K^+p \rightarrow K^+p} = \frac{a_0 + a_1 p + a_2 p^2}{1 + a_3 p + a_4 p^2} \quad , \tag{A1}$$

where p denotes the kaon momentum in the rest frame of the nucleon and we use: $a_0 = 10.508$ mb, $a_1 = -3.716$ mb/GeV, $a_2 = 1.845$ mb/GeV^2, $a_3 = -0.764$/GeV, $a_4 = 0.508$/GeV^2. In Fig. 15 (upper part) we show that this gives a good description of the experimental data. For scattering on a neutron there exist in the relevant energy range only a few experimental data for the charge exchange process $K^+ n \to K^0 p$ [37] and no data for the process $K^+ n \to K^+ n$. Therefore, we assume on the neutron the same total elastic cross section (including charge exchange):

$$\sigma_{K^+ n \to K^+ n} = \sigma_{K^+ n \to K^0 p} = \frac{1}{2}\sigma_{K^+ p \to K^+ p}.$$

This is a rather crude approximation which is also not in line with the experimental data for $K^+ n \to K^0 p$ at low momenta [37]. However, for the calculations presented here this is not essential since all these cross sections are small and, in particular, for low momenta they play only a small role for the phase space distributions of the particles involved.

The inelastic kaon-nucleon cross section is obtained by a spline interpolation through selected data points of the total cross section after subtraction of the elastic contribution. The resulting cross sections are displayed in Fig. 15 (middle part for $K^+ p$, lower part for $K^+ n$). We assume the inelastic cross section to consist only of $K\pi N$ states which is a good approximation since these cross sections are only used for invariant collision energies below 2.2 GeV. The cross sections for K^0 scattering on nucleons follow from isospin symmetry:

$$\sigma_{K^0 p} = \sigma_{K^+ n}, \quad \sigma_{K^0 n} = \sigma_{K^+ p}.$$

In case of antikaon scattering on nucleons we first get contributions to the cross sections from the $S = -1$ resonances listed above which we treat analogous to pion-nucleon scattering [16] as incoherent Breit-Wigner type contributions. From Fig. 16 one sees that these contributions alone – unlike the case of pion-nucleon – do not suffice to describe the cross sections for the different channels. Therefore we have introduced a non-resonant background cross section of the following form for the different channels i in $K^- p$ scattering:

$$\sigma^{bg}_{K^- p \to i} = a_0 \frac{p_f}{p_i s} \left(\frac{a_1^2}{a_1^2 + p_f^2} \right)^{a_2} , \tag{A2}$$

where p_i and p_f denote the cms momenta of the initial and final particles, respectively and $\sqrt{s}$ is the total cms energy. The parameters a_j are given in Table II. For $K^- p \to K^- p$ this parameterization is only used for invariant energies below 1.7 GeV. For larger energies we use a spline interpolation through selected experimental data points because the broad bump in the experimental data around 1.8 GeV can hardly be described by a simple fit function. From Fig. 16 one sees that our parameterizations give a good description of the experimental data for $K^- p \to K^- p, K^0 n, \Lambda\pi^0, \Sigma^+\pi^-, \Sigma^-\pi^+, \Sigma^0\pi^0$.

In order to describe the total $K^- p$ cross section in the relevant energy range it is necessary to also include channels with more than 2 particles in the final state. This is done here by including the process $\bar{K} N \to Y^* \pi$ with a constant matrix element for all hyperon resonances. The cross section is then given as:

$$\sigma_{\bar{K} N \to Y^* \pi} = C \frac{|\mathcal{M}|^2}{p_i s} \int^{\sqrt{s} - m_\pi} d\mu \, p_f \mathcal{A}_{Y^*}(\mu) , \tag{A3}$$

10

where the isospin factor C is given by the following expression of Clebsch-Gordan coefficients:

$$C = \sum_I \left(\langle \frac{1}{2}\frac{1}{2} I_{z,\bar{K}} I_{z,N} | \frac{1}{2}\frac{1}{2} I I_{z,tot} \rangle \langle I_{Y^*} 1 I_{z,Y^*} I_{z,\pi} | I_{Y^*} 1 I I_{z,tot} \rangle \right)^2. \tag{A4}$$

In Eq. (A3) $\mathcal{A}_{Y^*}$ stands for the spectral function of the hyperon resonance Y^* that is treated analogous to the ones for the nucleonic resonances [16]. For the squared matrix element we use $|\mathcal{M}|^2 = 22$ mb GeV^2 and we take for this process only the hyperon resonances into account with a mass above 1.6 GeV. In Fig. 17 (upper part) we show that the sum of all partial contributions very well describes the total $K^- p$ cross section.

For $K^- n$ scattering the elastic scattering cross section can be described by the resonance contributions with a small constant background cross section:

$$\sigma^{bg}_{K^- n \to K^- n} = 4 \text{ mb}.$$

The cross section for $K^- n \to \Lambda \pi^-$ follows from isospin symmetry from $K^- p \to \Lambda \pi^0$:

$$\sigma_{K^- n \to \Lambda \pi^-} = 2\sigma_{K^- p \to \Lambda \pi^0}.$$

In the $\Sigma \pi$ channel we have from isospin symmetry:

$$\sigma_{K^- n \to \Sigma^- \pi^0} = \sigma_{K^- n \to \Sigma^0 \pi^-}$$

and for the non-resonant background we assume:

$$\sigma^{bg}_{K^- n \to \Sigma^- \pi^0} = \frac{1}{2} \left(\sigma^{bg}_{K^- p \to \Sigma^- \pi^+} + \sigma^{bg}_{K^- p \to \Sigma^+ \pi^-} \right).$$

This is a rather crude approximation. However, for the calculations presented here it is only of primary importance that the total cross section, summed over all final states, are correctly described. The result for the total $K^- n$ cross section is displayed in Fig. 17 (lower part) and one sees that the available experimental data are reasonably well reproduced. The cross sections for $\bar{K}^0$ scattering on nucleons immediately follow from isospin symmetry:

$$\sigma_{\bar{K}^0 p} = \sigma_{K^- n}, \quad \sigma_{\bar{K}^0 n} = \sigma_{K^- p}.$$

APPENDIX B: STRANGENESS PRODUCTION IN PHOTON-NUCLEON COLLISIONS

The exclusive strangeness production processes $\gamma N \to \Lambda K, \Sigma K, N K \bar{K}$ are fitted to available experimental data. The channel YK is parameterized by the following expression:

$$\sigma_{\gamma N \to YK} = a_0 \frac{p_f}{p_i s} \frac{a_1^2}{a_1^2 + (\sqrt{s} - \sqrt{s_0})^2} \quad , \tag{B1}$$

where $\sqrt{s_0}$ denotes the invariant threshold energy. We assume the constants a_0 and a_1 to be independent of the isospin states of the incoming and outgoing particles and use: $a_0^\Lambda = 13$

μbGeV^2, $a_0^\Sigma = 15$ μbGeV^2, $a_1^\Lambda = 0.5$ GeV, $a_1^\Sigma = 0.4$ GeV. In Fig. 18 it is shown that these parameterizations describe the experimental data reasonably well.

The cross section for antikaon production $\gamma N \to NK\bar{K}$ is parameterized by:

$$\sigma_{\gamma N \to NK\bar{K}} = a_0 \frac{16(2\pi)^7}{p_i\sqrt{s}} \Phi_3 \frac{a_1^2}{a_1^2 + (\sqrt{s} - \sqrt{s_0})^2} \quad , \tag{B2}$$

where Φ_3 denotes the 3-body phase space as, for example, given by Eq. (35.11) in Ref. [24]. From the experimental data for $\gamma p \to pK^+K^-$ we obtain $a_0 = 12$ μb and $a_1 = 0.7$ GeV (resulting cross section shown in Fig. 18). These values are used for all isospin channels.

In Fig. 19 we compare our treatment of strangeness production in photon-proton reactions to the available experimental data on inclusive strangeness production. The dashed line shows the sum of the exclusive processes $\gamma p \to \Lambda K, \Sigma K, NK\bar{K}$; the dotted line is the strangeness production cross section that results from the string fragmentation model FRITIOF. We note that the string fragmentation model does not produce the exclusive channels such that there is no double counting involved here. The total inclusive strangeness production cross section, as sum of the contributions from the exclusive channels and the string model, is displayed as solid line in Fig. 19. The experimental data are described rather well up to a photon energy of 4 GeV, but for larger energies the experimental cross section is overestimated by about 50%. The experimental data seem to indicate a saturation of the cross section already at 4 GeV which is hard to explain. Therefore we use the described cross sections keeping in mind that out treatment of the elementary photon-nucleon reaction might need to be refined when new and more reliable experimental data will become available.

REFERENCES

[1] V. Muccifora et al., Phys. Rev. C **60** (1999) 064616.

[2] N. Bianchi, E. De Sanctis, M. Mirazita, V. Muccifora, Phys. Rev. C **60** (1999) 064617.

[3] U. Mosel, Ann. Rev. Nucl. Part. Sci. **41**, 29 (1991).

[4] C.M. Ko, V. Koch, and G.Q. Li, Ann. Rev. Nucl. Part. Sci. **47**, 505 (1997).

[5] G. Agakichiev et al., Phys. Rev. Lett. **75**, 1272 (1995).

[6] M. A. Mazzoni, Nucl. Phys. A **566**, 95c (1994); M. Masera, Nucl. Phys. A **590**, 93c (1995).

[7] G.Q. Li, C.M. Ko, G.E. Brown, H. Sorge, Nucl. Phys. A **611**, 539 (1996).

[8] W. Cassing and E. L. Bratkovskaya, Phys. Rep. **308**, 65 (1999).

[9] M. Effenberger, A. Hombach, S. Teis, U. Mosel, Nucl. Phys. A **613**, 353 (1997).

[10] W. Peters, M. Post, H. Lenske, S. Leupold, U. Mosel, Nucl. Phys. A **632**, 109 (1998).

[11] S. Teis, W. Cassing, M. Effenberger, A. Hombach, U. Mosel, and Gy. Wolf, Z. Phys. A **356**, 421 (1997).

[12] A. Hombach, W. Cassing, S. Teis, U. Mosel, Eur. Phys. J. A **5**, 157 (1999).

[13] M. Effenberger, A. Hombach, S. Teis, U. Mosel, Nucl. Phys. A **614**, 501 (1997).

[14] M. Effenberger, E.L. Bratkovskaya, W. Cassing, and U. Mosel, Phys. Rev. C **60**, 27601 (1999).

[15] The HADES collaboration, Proposal for a High Acceptance Dielectron Spectrometer, GSI 1994.

[16] M. Effenberger, E.L. Bratkovskaya, U. Mosel, Phys. Rev. C **60**, 44614 (1999).

[17] P. Bertin et al., CEBAF proposal E94002.

[18] J. Lehr, M. Effenberger, and U. Mosel, nucl-th/9907091, Nucl. Phys. A (2000), in press.

[19] T.H. Bauer, R.D. Spital, D.R. Yennie, and F.M. Pipkin, Rev. Mod. Phys. **50**, 261 (1978), Erratum **51**, 407 (1979).

[20] A. M. Boyarski et al., Phys. Rev. Lett. **23**, 1343 (1969).

[21] W. T. Meyer et al., Phys. Rev. Lett. **28**, 1344 (1972).

[22] G. McClellan et al., Phys. Rev. Lett. **23**, 554 (1969).

[23] D. M. Manley and E. M. Saleski, Phys. Rev. D **45**, 4002 (1992).

[24] Particle Data Group, Eur. Phys. J. C **3**, 1 (1998).

[25] B. Anderson, G. Gustafson and Hong Pi, Z. Phys. C **57**, 485 (1993).

[26] K. Tsushima, S.W. Huang, and A. Faessler, Austral. J. Phys. **50**, 35 (1997).

[27] A. Sibirtsev, W. Cassing, and C.M. Ko, Z. Phys. A **358**, 101 (1997).

[28] J. Schaffner-Bielich, V. Koch, and M. Effenberger, nucl-th/9907095, Nucl. Phys. A (2000) in press.

[29] Baldini et al., *Landolt-Börnstein*, Band 12, Springer Verlag, Berlin, 1987.

[30] M.Q. Tran et al., Phys. Lett. B **445**, 20 (1998).

[31] D.O. Caldwell, V.B. Elings, W.P. Hesse, R.J. Morrison, and F.V. Murphy, Phys. Rev. D **7**, 1362 (1973).

[32] V. Heynen, H. Meyer, B. Naroska, and D. Notz, Phys. Lett. B **34**, 651 (1971).

[33] G.R. Brookes et al., Phys. Rev. D **8**, 2826 (1973).

[34] Particle Data Group, Phys. Rev. D **50**, 1 (1994).

[35] G.E. Brown and M. Rho, Phys. Rev. Lett. **66**, 2720 (1991).

[36] T. Hatsuda and S. Lee, Phys. Rev. C **46**, R34 (1992).

[37] R.G. Glasser et al., Phys. Rev. D **15**, 1200 (1977).

TABLES

Y(M_0/MeV)	Γ_0 [MeV]	J^P	branching ratios [%]						
			$\Lambda\pi$	$N\bar{K}$	$\Sigma\pi$	$\Sigma^*\pi$	$\Lambda\eta$	$N\bar{K}^*$	$\Lambda^*\pi$
$\Lambda(1116)$	0	$\frac{1}{2}^+$	0	0	0	0	0	0	0
$\Sigma(1189)$	0	$\frac{1}{2}^+$	0	0	0	0	0	0	0
$\Sigma(1385)$	36	$\frac{3}{2}^+$	88	0	12	0	0	0	0
$\Lambda(1405)$	50	$\frac{1}{2}^-$	0	0	100	0	0	0	0
$\Lambda(1520)$	16	$\frac{3}{2}^-$	0	46	43	11	0	0	0
$\Lambda(1600)$	150	$\frac{1}{2}^+$	0	35	65	0	0	0	0
$\Sigma(1660)$	100	$\frac{1}{2}^+$	40	20	40	0	0	0	0
$\Lambda(1670)$	35	$\frac{1}{2}^-$	0	25	45	0	30	0	0
$\Sigma(1670)$	60	$\frac{3}{2}^-$	15	15	70	0	0	0	0
$\Lambda(1690)$	60	$\frac{3}{2}^+$	0	25	30	45	0	0	0
$\Sigma(1750)$	90	$\frac{1}{2}^-$	10	30	60	0	0	0	0
$\Sigma(1775)$	120	$\frac{5}{2}^-$	20	45	5	10	0	0	20
$\Lambda(1800)$	300	$\frac{1}{2}^-$	0	35	35	30	0	0	0
$\Lambda(1810)$	150	$\frac{1}{2}^+$	0	35	20	0	0	45	0
$\Lambda(1820)$	80	$\frac{5}{2}^+$	0	60	12	28	0	0	0
$\Lambda(1830)$	95	$\frac{5}{2}^-$	0	5	60	35	0	0	0
$\Lambda(1890)$	100	$\frac{3}{2}^+$	0	30	10	30	0	30	0
$\Sigma(1915)$	120	$\frac{5}{2}^+$	45	10	45	0	0	0	0
$\Sigma(2030)$	180	$\frac{7}{2}^+$	25	25	10	15	0	5	20
$\Lambda(2100)$	200	$\frac{7}{2}^-$	0	30	5	45	0	20	0
$\Lambda(2110)$	200	$\frac{5}{2}^+$	0	15	30	0	0	55	0

TABLE I. Properties of $S = -1$ resonances. M_0 and Γ_0 denote the pole mass and the width at the pole mass, respectively.

channel	a_0[mb GeV^2]	a_1[GeV]	a_2
K^-p	150	0.35	2
$\bar{K}^0n$	100	0.15	2
$\Lambda\pi^0$	130	0.25	3
$\Sigma^+\pi^-$	600	0.1	2
$\Sigma^-\pi^+$	5000	0.1	3
$\Sigma^+\pi^-$	2500	0.1	3

TABLE II. Parameters for cross sections in K^-p scattering used for Eq. (A2).

FIGURES
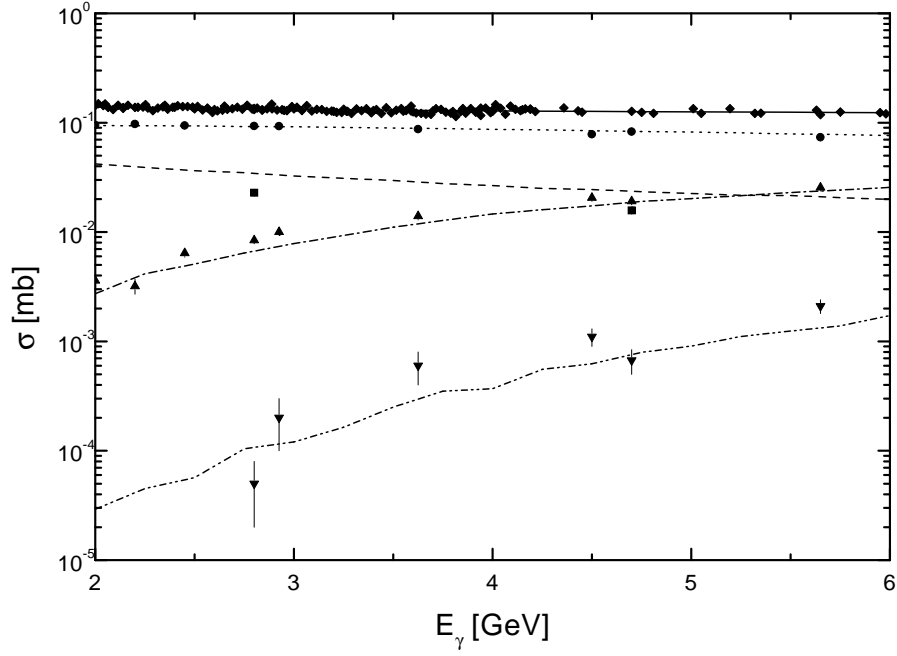
FIG. 1. Charged particle multiplicity cross sections in γp reactions: $\gamma p \rightarrow 1$ charged particle (dashed line (calculation as described in the text), squares (experimental data from Ref. [29])), 3 charged particles (dotted line, circles), 5 charged particles (dot-dashed line, up triangles), 7 charged particles (dot-dot-dashed line, down triangles). Also shown is the total cross section (solid line, rhombs).
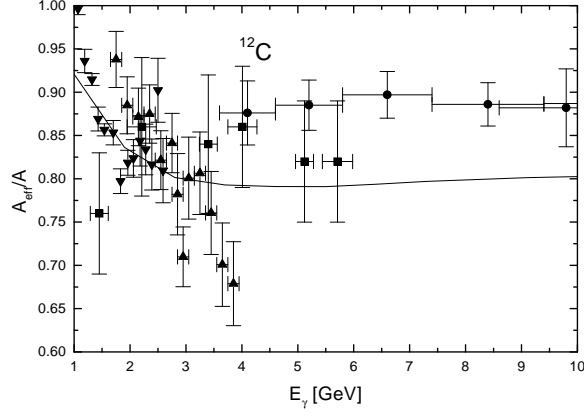
FIG. 2. Effective mass number as function of photon energy for photoabsorption on ^{12}C. The experimental data are taken from Refs. [31] (circles), [32] (squares), [33] (up triangles), [1] (down triangles). The latter two are obtained from the experimental data on the total cross sections by using the parameterization of the cross section on a single nucleon from Ref. [34].
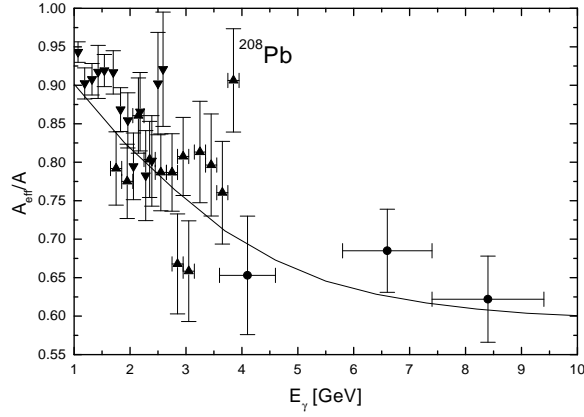
FIG. 3. Effective mass number as function of photon energy for photoabsorption on ^{208}Pb. See Fig. 2 for references to the experimental data.

16
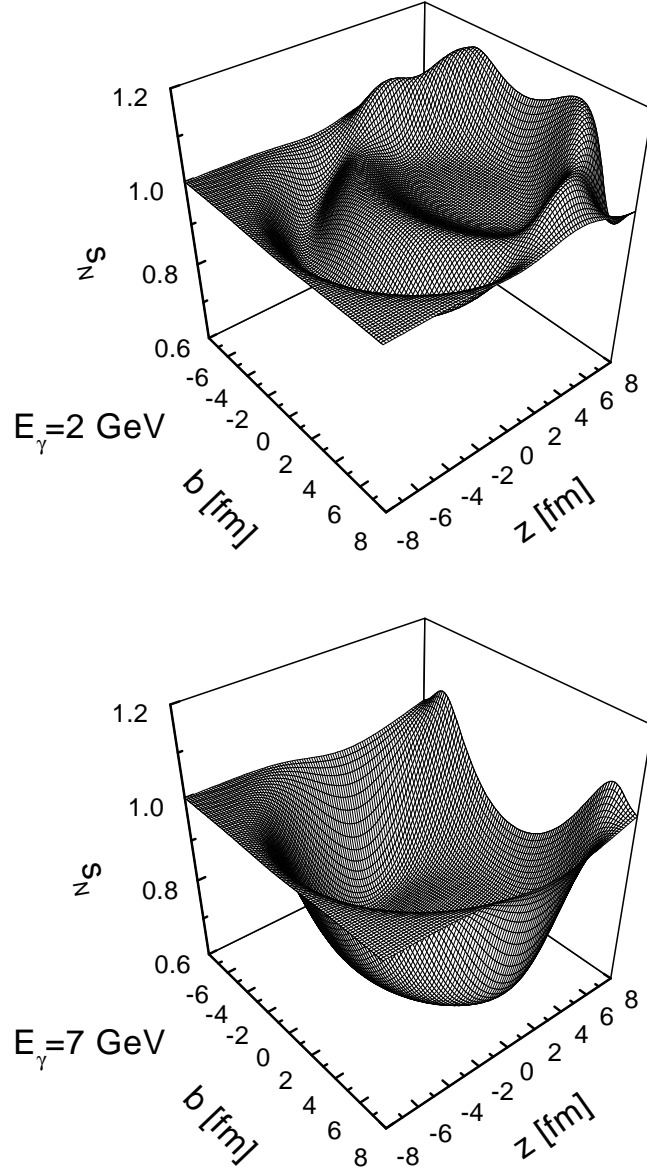
FIG. 4. Coordinate dependence of the shadowing factor s_N for a γPb reaction at 2 GeV (upper part) and 7 GeV (lower part).
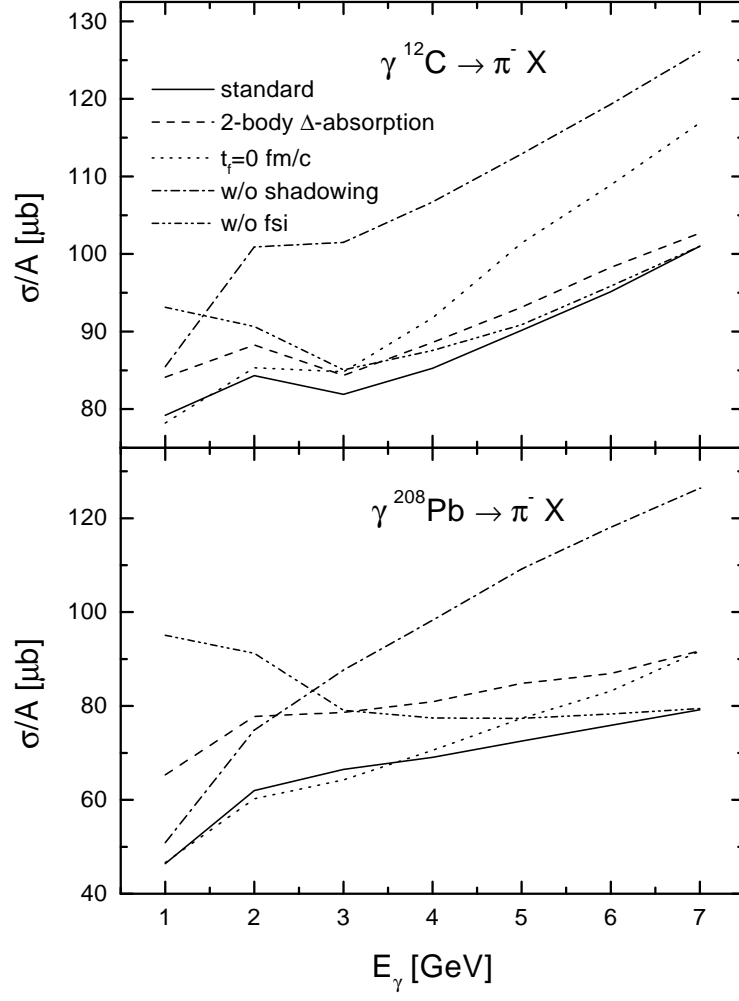
FIG. 5. Total cross sections for π^--production in γC (upper part) and γPb (lower part) reactions. See text for a detailed explanation of the different lines.

18
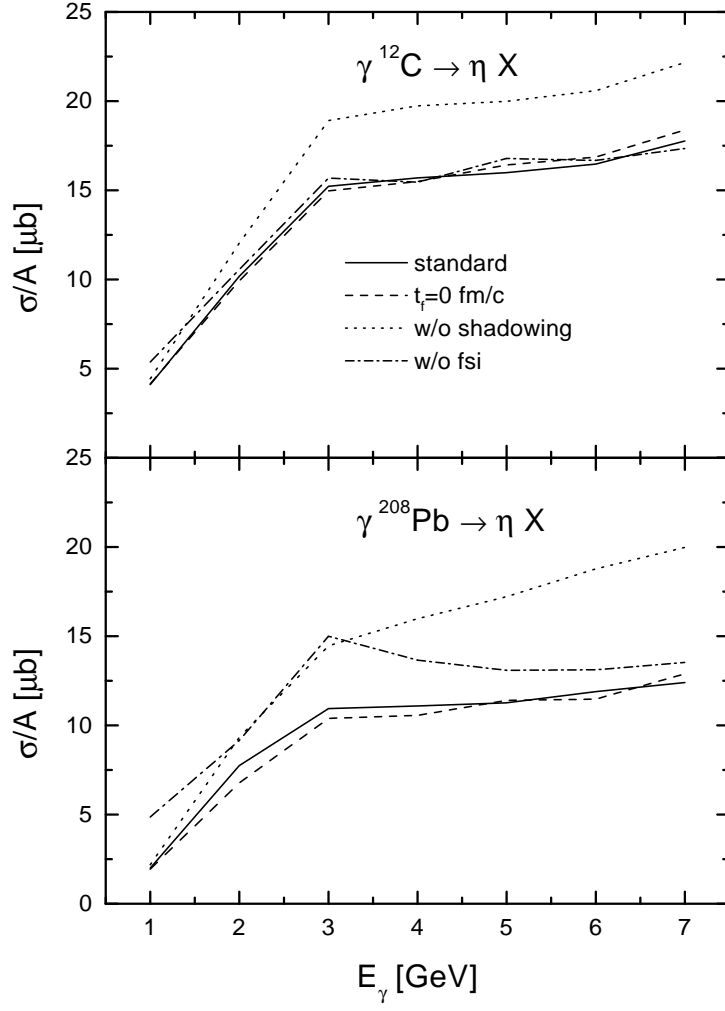
FIG. 6. Total cross sections for η-production in γC (upper part) and γPb (lower part) reactions. See text for a detailed explanation of the different lines.
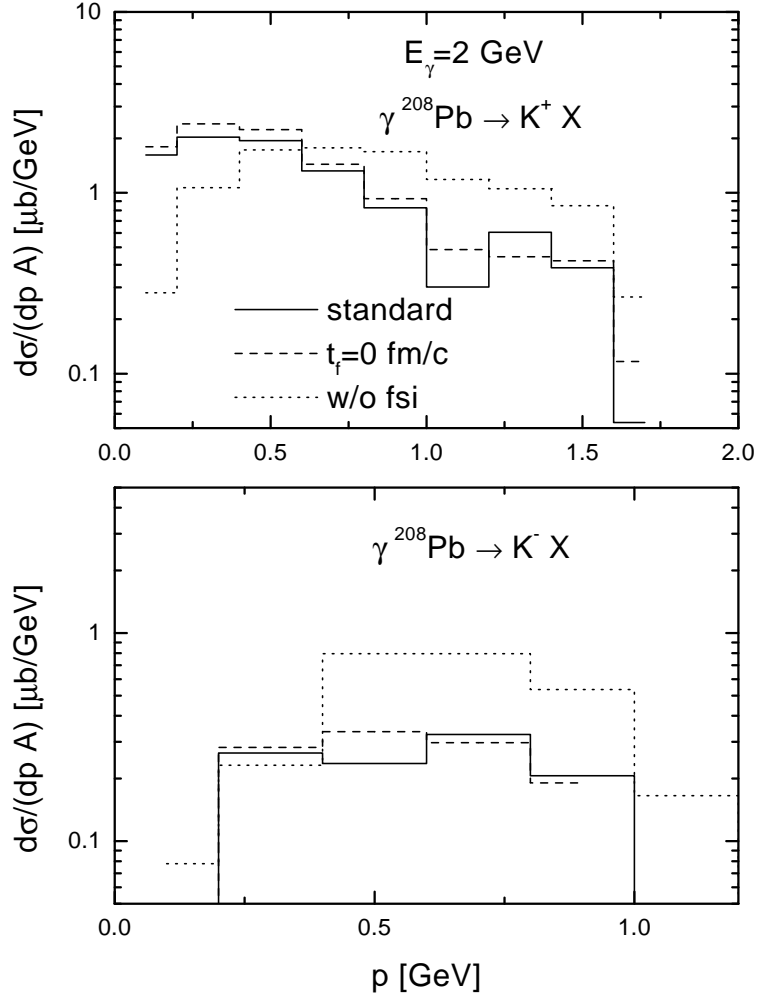
19
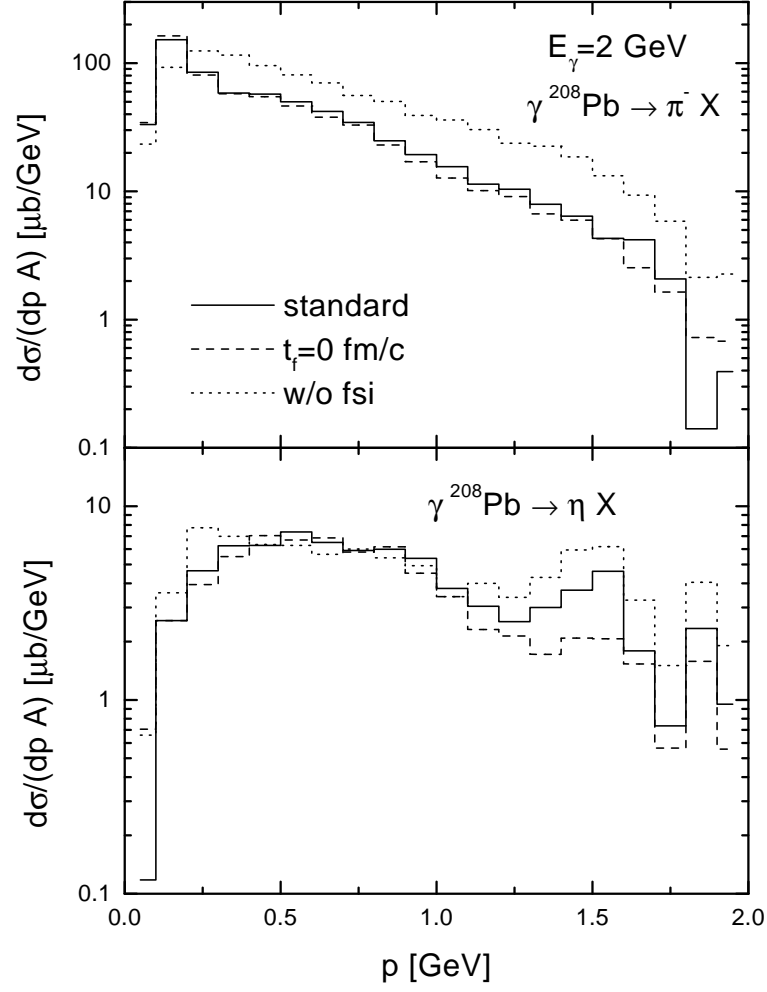
FIG. 7. Momentum differential cross sections for π^- (upper part) and η (lower part) production in γPb reactions at a photon energy of $E_\gamma = 2$ GeV.
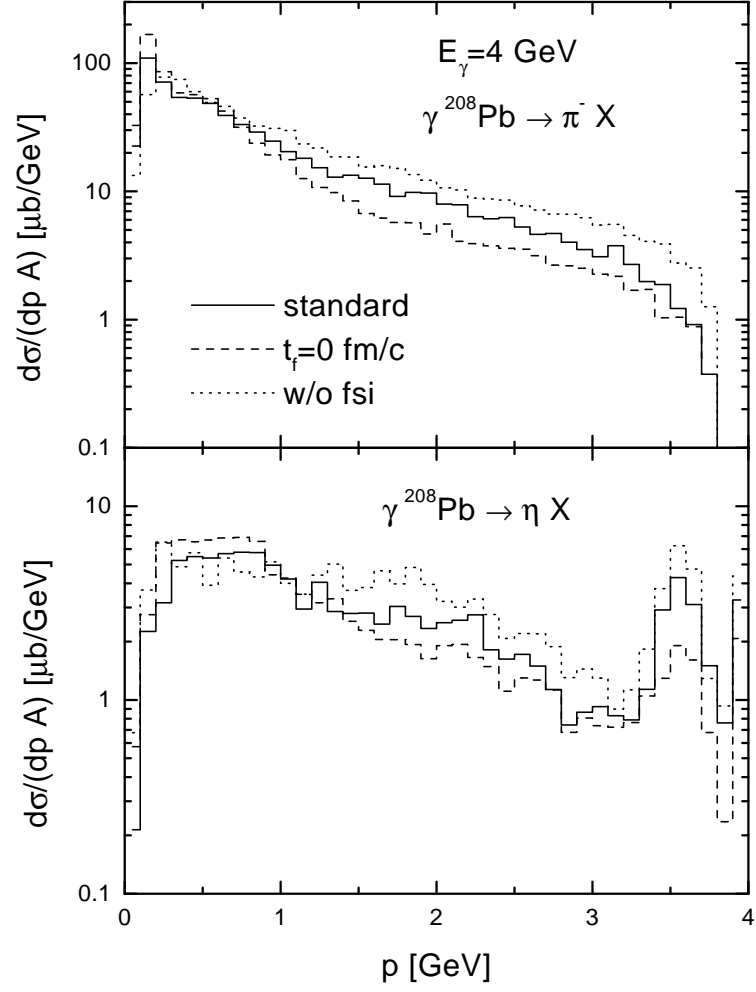
FIG. 8. Momentum differential cross sections for π^- (upper part) and η (lower part) production in γPb reactions at a photon energy of $E_\gamma = 4$ GeV.
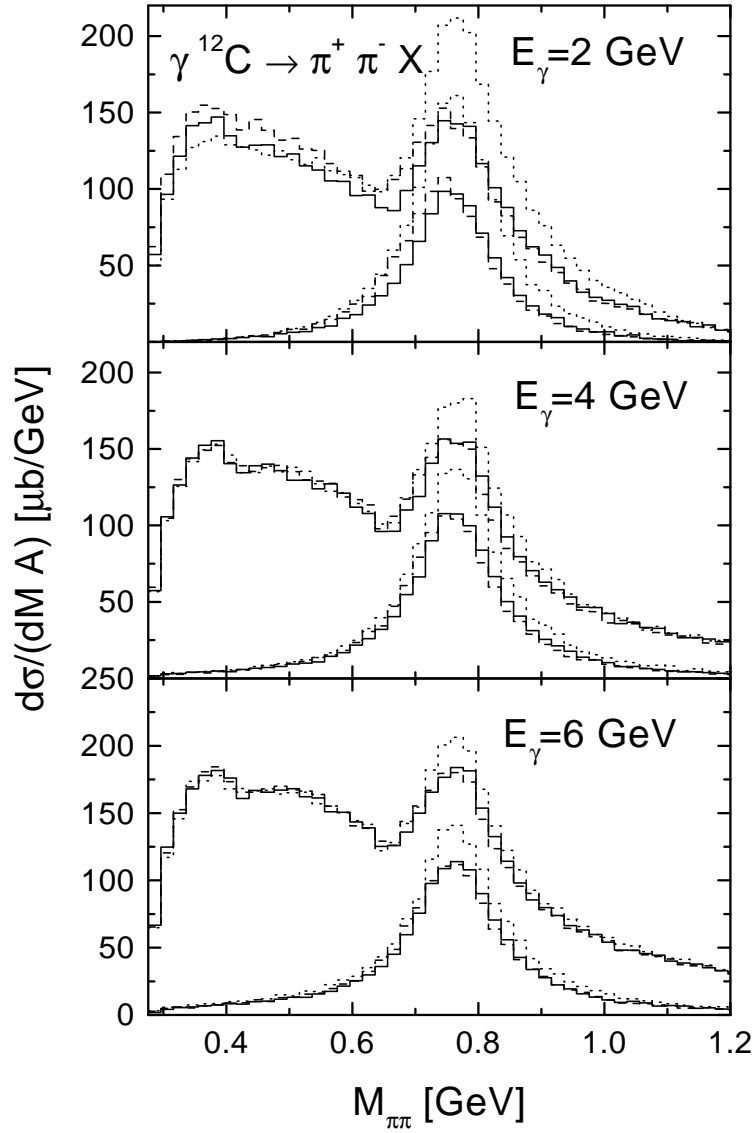
FIG. 9. Invariant mass spectrum of inclusive $\pi^+\pi^-$ production in γC reactions. The dashed lines are the results with a dropping mass scenario for the ρ meson. The dotted lines result without final state interactions. The total mass differential cross sections as well as the contributions coming from the ρ meson are displayed.
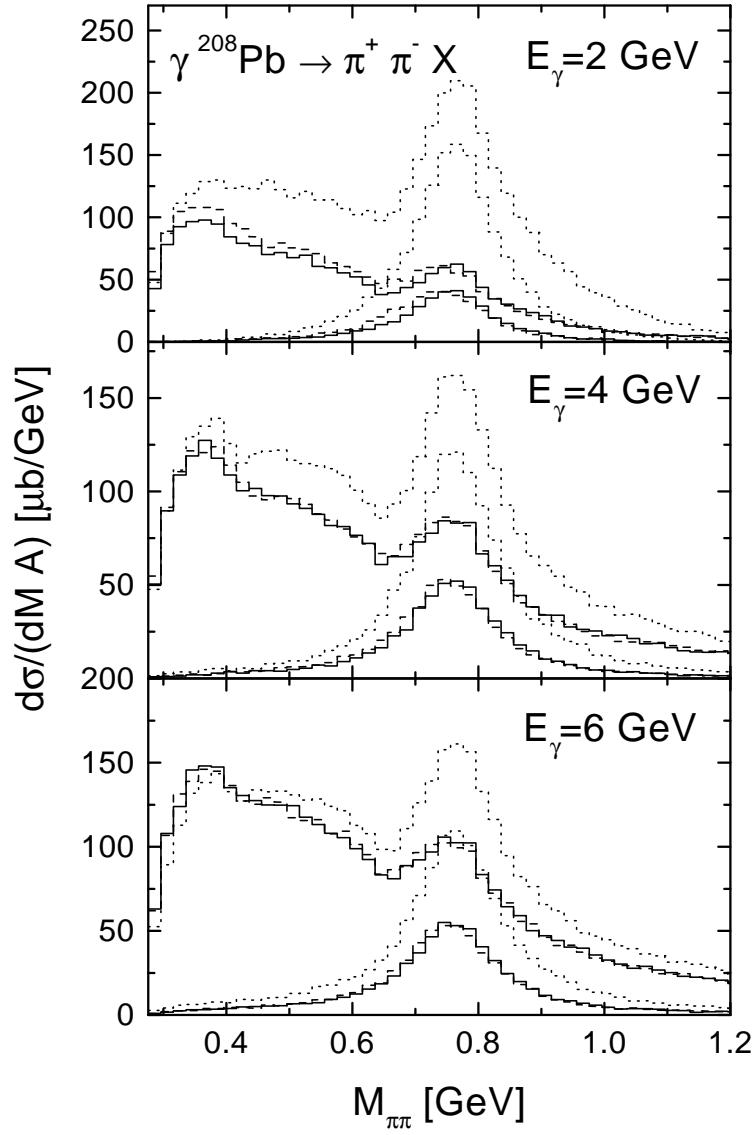
FIG. 10.   Same as Fig. 9 for γPb reactions.

23
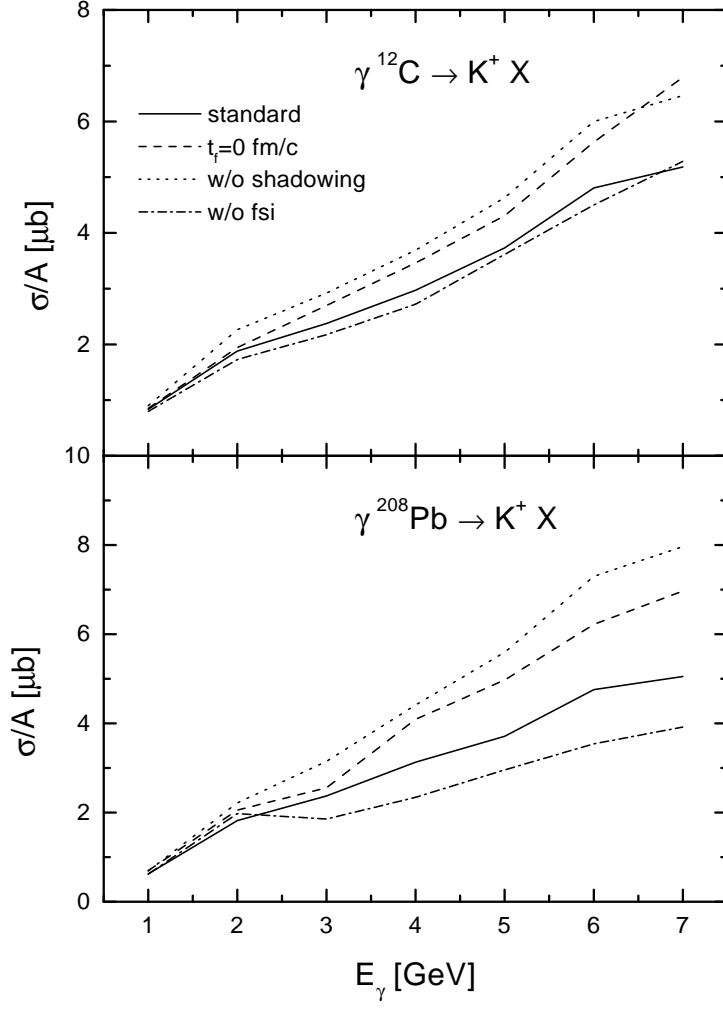
FIG. 11. Total cross sections for K^+-production in γC (upper part) and γPb (lower part) reactions.
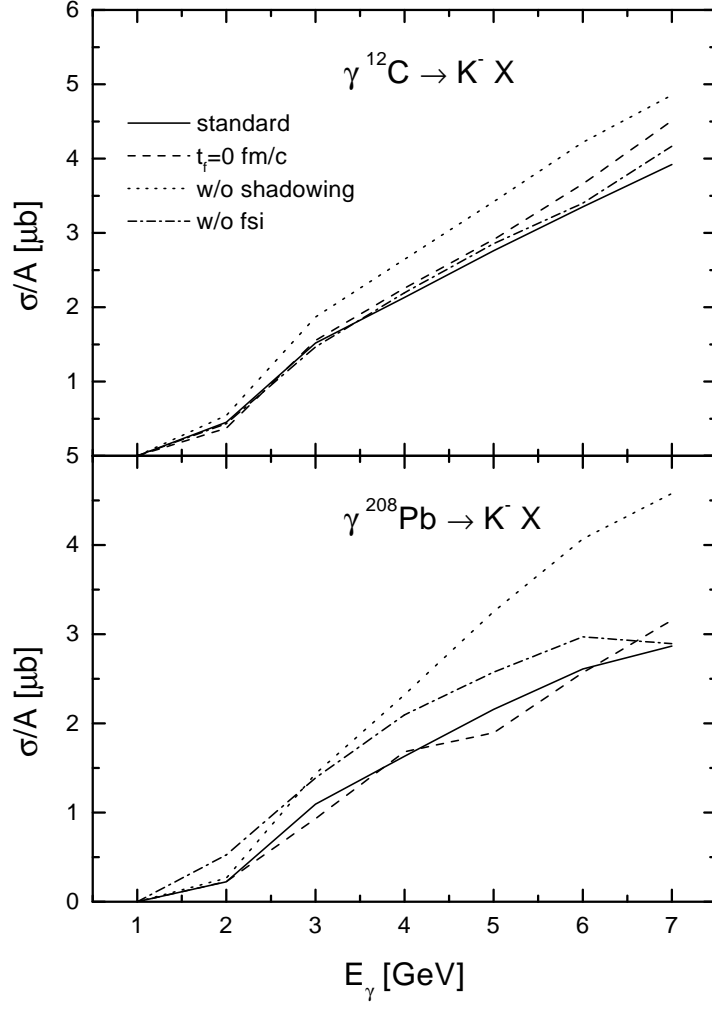
FIG. 12. Total cross sections for K^--production in γC (upper part) and γPb (lower part) reactions.

FIG. 13. Momentum differential cross sections for K^+ (upper part) and K^- (lower part) production in γPb reactions at a photon energy of $E_\gamma = 2$ GeV.
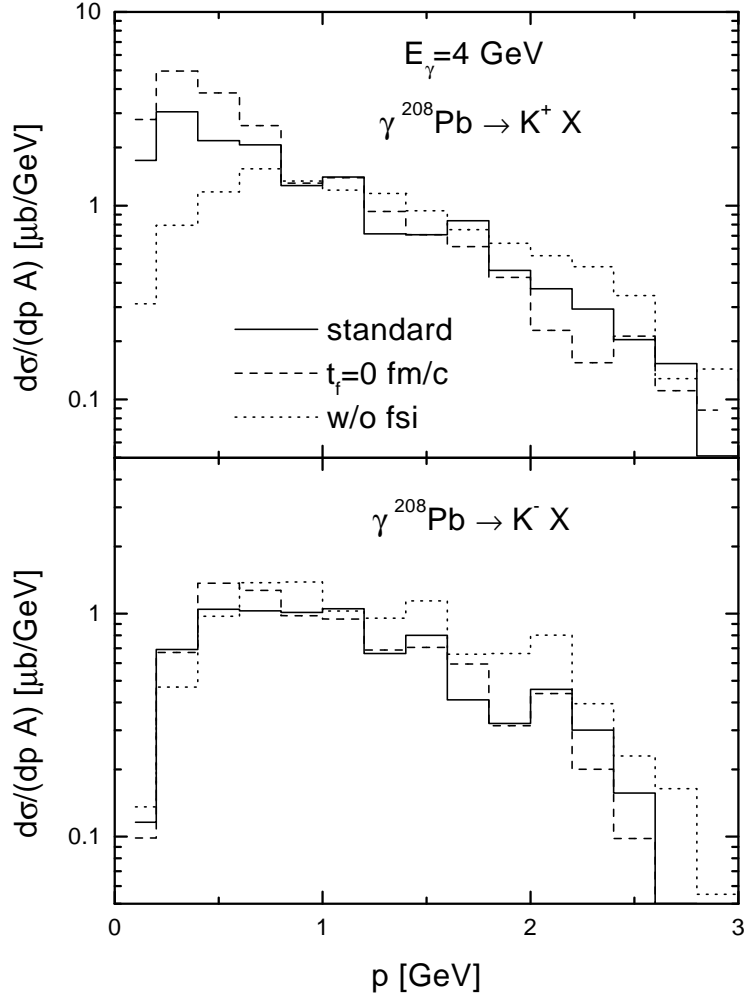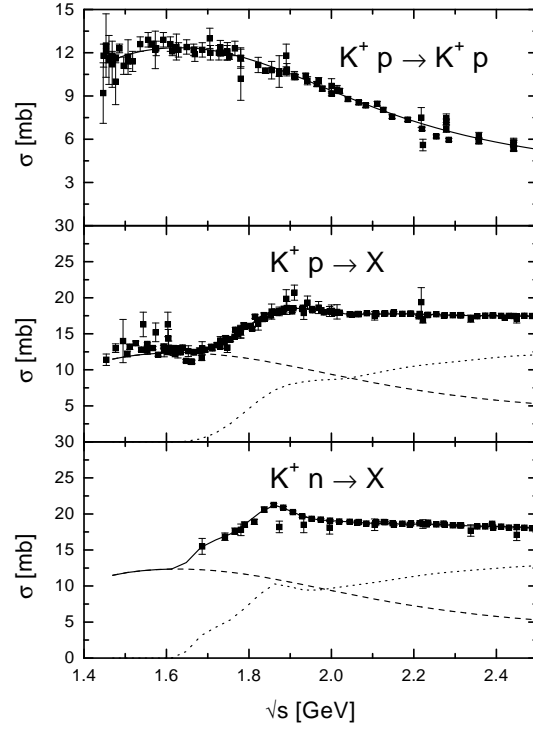
FIG. 14. Momentum differential cross sections for K^+ (upper part) and K^- (lower part) production in γPb reactions at a photon energy of $E_\gamma = 4$ GeV.

FIG. 15. Parameterizations of the elastic K^+p scattering cross section (upper part), the total K^+p cross section (middle part), and the total K^+n cross section (lower part) as compared to the experimental data from [29]. In the plots of the total cross sections the dashed and the dotted lines show the elastic and the inelastic contributions, respectively.
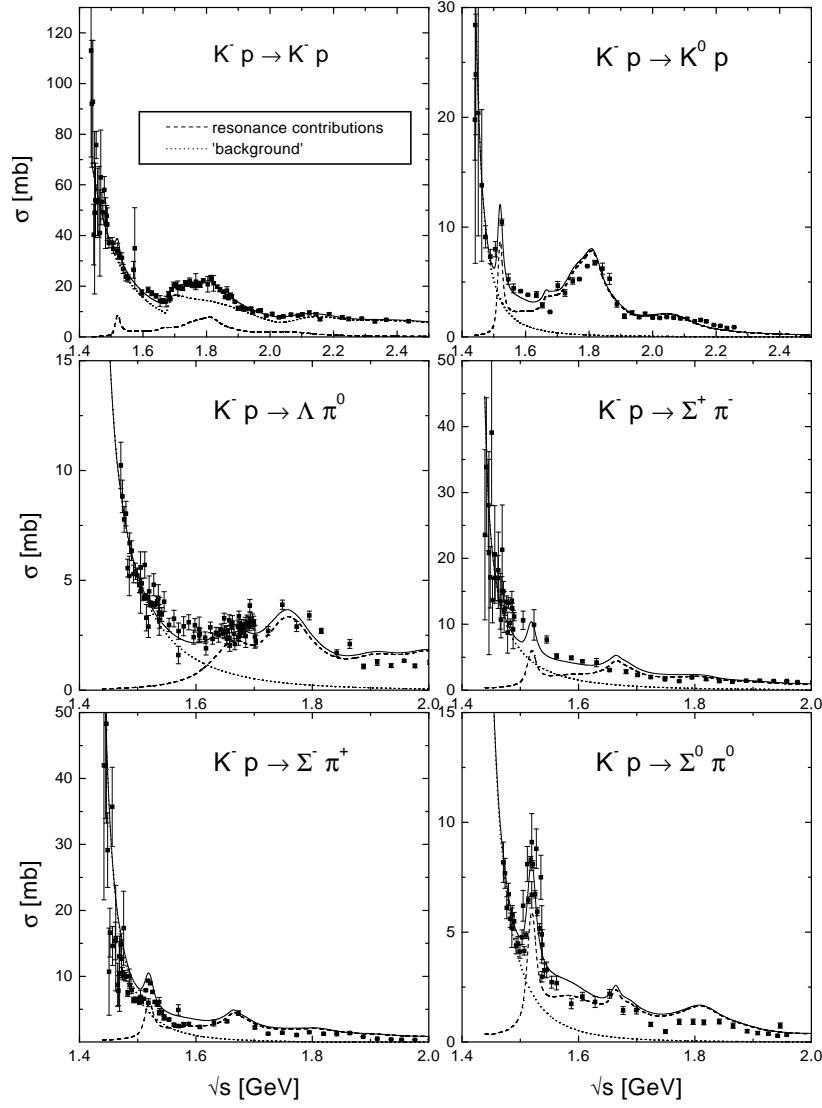
FIG. 16. Cross sections for elastic scattering, charge exchange, and hyperon production reactions in K^-p collisions. We show the total calculated cross sections (solid lines), the resonance contributions (dashed lines), and the parameterizations of the non-resonant background (dotted lines). The experimental data are taken from [29].
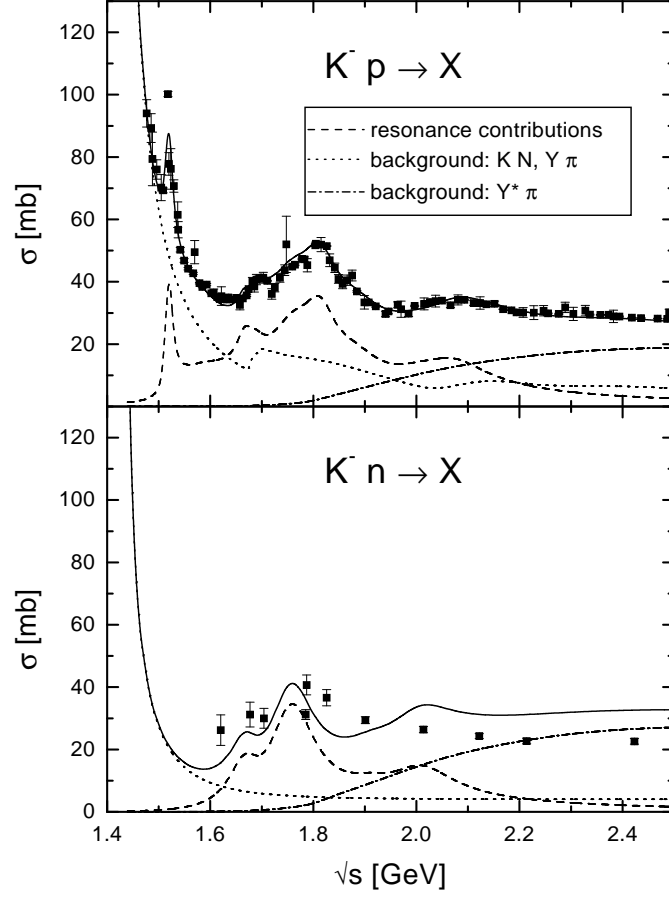
FIG. 17. Total cross sections (solid lines) for K^-p (upper part) and K^-n (lower part) collisions and the different contributions: Resonance contributions (dashed lines), non-resonant $\bar{K}N$ and $Y\pi$ contributions (dotted lines), and $Y^*\pi$ contributions (dash-dotted lines). The experimental data are taken from [29].
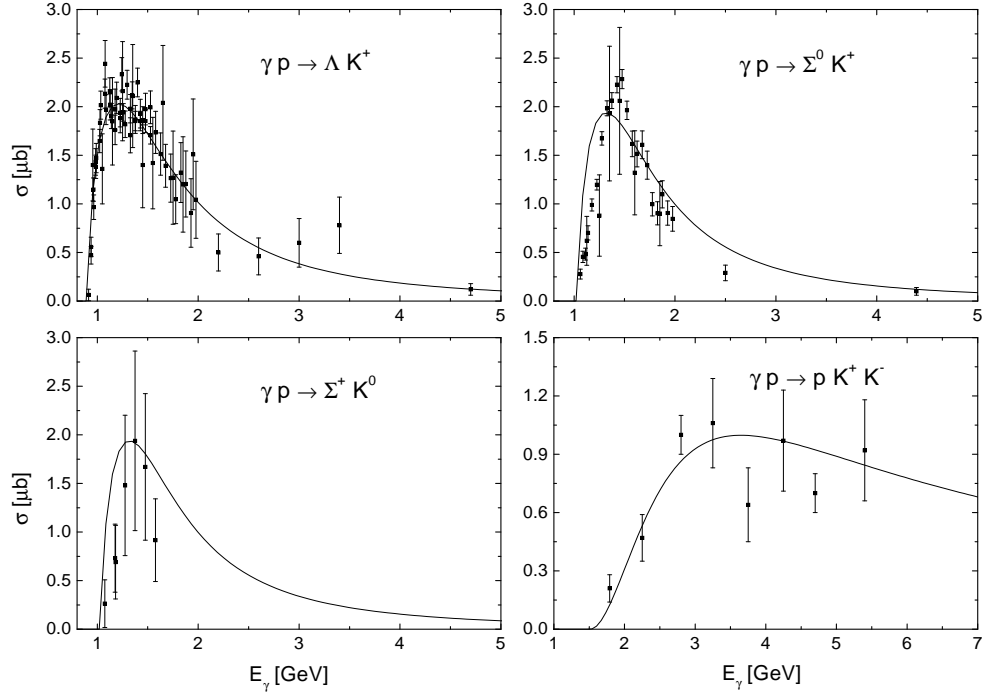
FIG. 18. Parameterizations of the cross sections for $\gamma p \to \Lambda K^+$, $\gamma p \to \Sigma^0 K^+$, $\gamma p \to \Sigma^+ K^0$, and $\gamma p \to pK^+K-$ compared to the experimental data from Refs. [29,30].
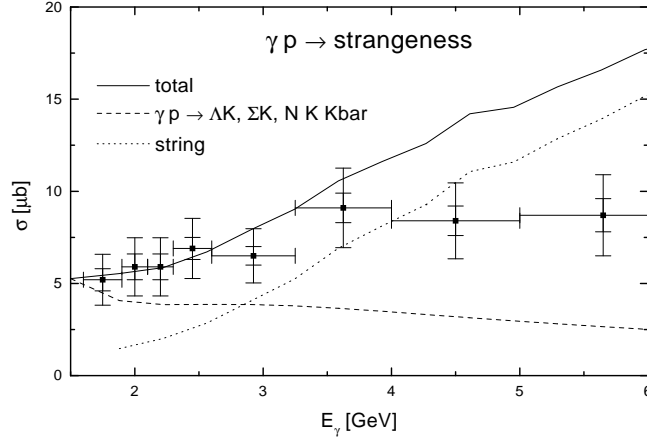

FIG. 19. Total cross section for strangeness production in γp reactions. Experimental data are taken from Ref. [29]. The inner error bar displays the statistical error, the outer one the sum of statistical and systematic error.